In-situ Observation of Damage Mechanisms by Digital Image Correlation during Tension and Low Cycle Fatigue of Magnesium alloys

A.A. Khan[1] and T.J. Marrow[2]

[1] *Pakistan Institute of Nuclear Science and Technology, (PINSTECH), Islamabad, Pakistan;**
[2] *School of Materials, The University of Manchester, UK;*

*(*visitor at The University of Manchester)*

ABSTRACT

A full field strain mapping technique based on digital image correlation analysis has been used to observe the surface strain fields during tensile and low cycle fatigue deformation of magnesium alloys Elektron WE43 and Elektron 21. Heterogeneous strain fields are obtained from localized deformation in the microstructure. The objective of this work is to correlate the locations of fatigue crack initiation and fatigue crack growth with intergranular strains and the distribution of microstructural features such as brittle intermetallic phases.

1 INTRODUCTION

Magnesium alloys are increasingly used for structural components [1]. It is therefore of interest to understand the role of microstructure in the development of damage, with the objective of alloy design for improved performance. Cast magnesium alloys, such as Elektron WE43 and Elektron 21 have quite low ductility, relative to aluminium alloys, and their low cycle fatigue resistance is therefore an important property [2].

In order to study damage nucleation, it is beneficial to be able to quantify the development of damage, and relate it to microstructure. The purpose of the this paper is to demonstrate the potential of a full field strain mapping techniques, digital image correlation, technique to evaluate the damage accumulation process in cast magnesium alloys. The distribution of deformation is related to the microstructures, which have been characterised prior to electron backscatter diffraction to measure grain orientations.

2 EXPERIMENTAL

The magnesium alloys WE-43 and Elektron 21 used for this work were provided by Magnesium Elektron Ltd. as cast plates, measuring 200mm × 200mm × 25 mm. Both were in the T6 condition (8 hours at 520°C, hot water quenched, 16 hours at 200°C for Elektron 21 and 8 hours at 525°C, hot water quenched, 16 hours at 250°C for Elektron WE43). The nominal chemical composition is given in Table 1. The tensile properties given in Table 2 are the average of three specimen tested. The test specimens are shown in Figure 1. They were designed to have a short gauge length (~4 mm), within which deformation and crack nucleation would be confined. The gauge length was electrolytically polished with a solution of 30% nitric acid/70% ethanol for 30 seconds at -30°C.

Table 1: Chemical Composition in Wt.%

	Zn	Cu	Fe	Ni	Zr	Nd	Y	Ag	Gd	Other RE	Others
Elektron 21	0.31	<0.001	0.003	<0.001	0.5	2.5		0.001	1.3	0.1	<0.01
WE 43					0.73	2.29	4.23			0.83	

Table 2: Mechanical Properties

	0.2% Proof Stress (MPa)	Tensile Strength (MPa)	Elongation (%)
Elektron 21	175	265	7
WE 43	180	265	7

Microstructural characterisaton of the gauge length was conducted by electron backscatter diffraction (EBSD) using a step size of 4μm to map an area of approximately 2 x 1.6 mm. An HKL-EBSD system with a low light CCD camera (Nordlys II), interfaced to a Cam Scan MaXim-SEM was used for this assessment. Data were acquired using Channel 5 Flamenco HKL software in the beam scanning mode, using an accelerating voltage of 20 kV and a 100 μm aperture. The acquisition time was set to 60 ms per point. The specimens were then lightly polished with OPS (aluminium oxide polishing solution) and electrolytically etched with a 10% aqueous solution of hydrofloric acid to provide features on the surface of specimen necessary for the application of digital image correlation.

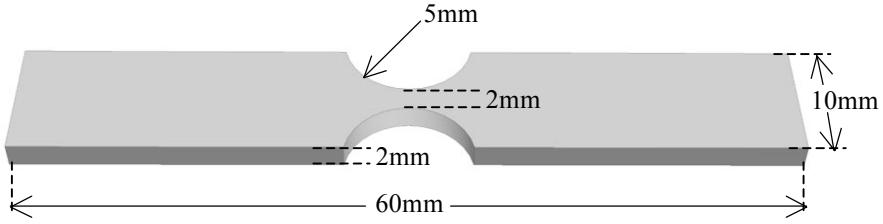

Figure 1: Fatigue specimen design

Load-controlled tension-tension low cycle fatigue tests were performed on a 2KN microtester (Deben MT10046) mounted on an Olympus BH2 optical microscope with a 1.36 Mega Pixel CCD camera (Carl Zeiss, Axio Cam MRm). The tests were conducted using a triangular waveform at a frequency of 1 cycle/min with a ratio (R) of minimum to maximum load of 0.25. The maximum stress (~250 MPa) was chosen to fracture the specimens within a few thousand cycles (i.e. low cycle fatigue).

Observations were made of an area of 2.2 mm ×1.8 mm at the centre of gauge section using a 5x objective lens. Micrographs were recorded at the maximum and minimum load of each cycle in the initial 10 cycles and then at after the peak loads every 10 cycles. The relative in-plane displacements and strains were calculated from these images by digital image correlation using LaVision Davis

software (Version 7.2), with a window size of 64 x 64 pixels and an overlap of 25%. One pixel was approximately 1.7 μm. The RMS (root mean square error) noise in displacement measurements was 0.008 pixels, which led to a noise in the strain measurement of approximately 0.005%. This did not vary significantly throughout the experiments.

3 RESULTS

The fatigue behaviour of the small specimens was variable, and differences in fatigue resistance of the two alloys have not been determined in this work. The initial surface of a WE43 sample is shown in Figure 2a. The small hardness indentations were used for locating the region of interest. The same sample surface is shown after 1510 cycles at a maximum stress of 256 MPa, and then after failure at 1513 cycles in Figure 2b and c. Deformation of the surface is apparent prior to failure. The approximate path of the crack is indicated. The EBSD map obtained prior to testing (colours indicate grain orientation, Euler) is shown in Figure 2d. The map of displacements between the images in Figure 2a and Figure 2b is shown in Figure 2e, relative to the image centre. The maximum displacement is approximately 25 pixels. The displacement vectors are observed to be predominantly parallel to the tensile axis, and there is a trend of increasing displacement magnitude across the viewed region. Simple inspection of the width of each contour shows that the gradient of displacement is not constant, and that strain is localised. Differentiation, to obtain the local displacement gradients between measurements, produces the strain map in Figure 2f. This shows the maximum normal strain from the 2D displacement vectors, but the highest magnitudes are primarily parallel to the tensile axis, which is horizontal in the image. Several regions of high strain (i.e. steeper gradients of displacement) are observed. Four such regions are indicated in the figure by arrows. The fracture path tended to follow the clustering of such regions (Figure 2f). No evidence was found for fatigue cracks in any of the optical images.

Similar observations for an Elektron 21 sample are shown in Figure 3. This sample failed at 552 cycles with a maximum stress of 248 MPa. There was less obvious deformation of the surface in the optical image (Figure 3b). However, strain localisation was also observed in the microstructure (Figure 3f), although the maximum magnitude was approximately half of that in WE43. The fracture path also tended to be associated with these regions. As for WE43, there was no evidence found for stable fatigue cracks in the optical images of the Elektron 21 samples.

Data for the variation of maximum normal strain with the number of cycles is summarised in Figure 4. The bulk strain is the maximum normal strain obtained with a differentiation over the whole observation window. It is the extension of the sample in the tensile direction. In both cases, it develops significantly over approximately the first 15 cycles, then increases more gradually with to a value of around 0.03 in WE43 and 0.02 in Elektron 21. The highest magnitude of the localised strain regions is approximately twice that of the bulk strain. In WE43, the localised strains reached a quite stable value after 60 to 1490 cycles,

increasing slightly again as before failure. In Elektron 21, the behaviour was similar, although some localised strains increased throughout the test, while others appeared stable.

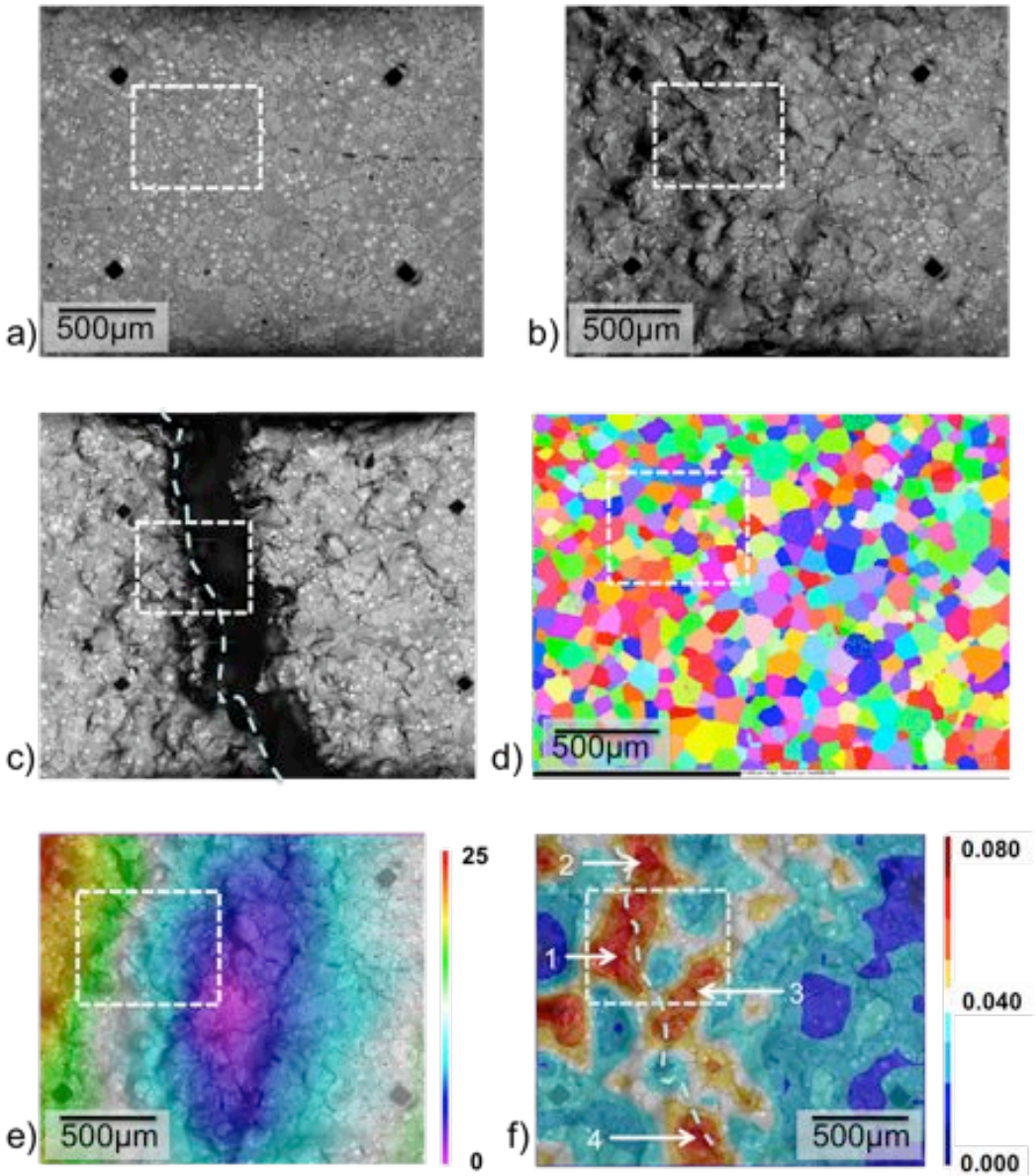

Figure 2: Observations for Elektron WE43, a) optical image of surface before fatigue, b) optical image after 1510 cycles, c) optical image after failure at 1513 cycles, d) EBSD map of sample obtained before testing, e) Displacement map between 0 and 1510 cycles, f) strain map between 0 and 1510 cycles. The same region is marked by a white dotted box in each image. Locations 1-4 in f) are examined in Figure 4. The loading direction in the images is horizontal.

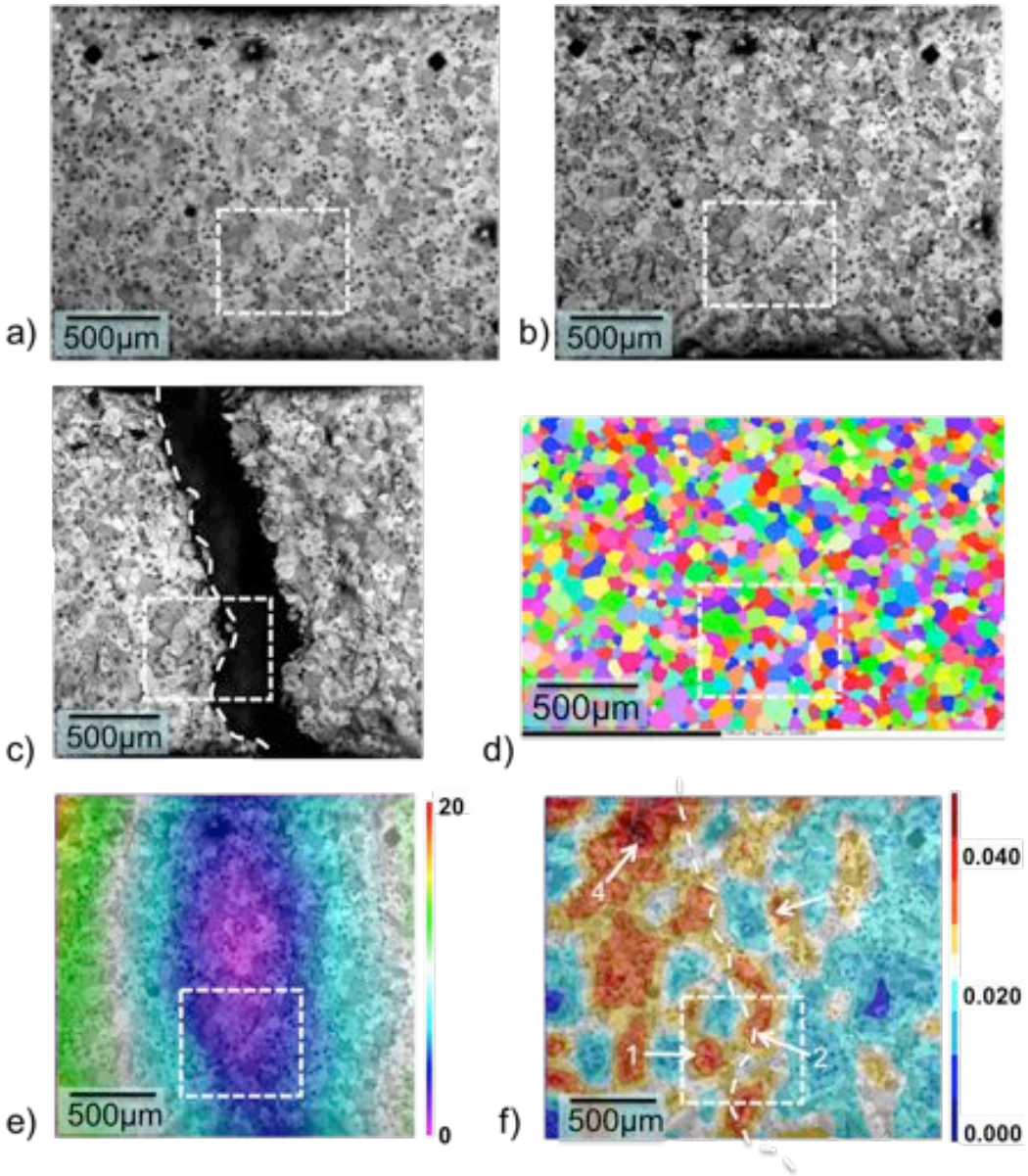

Figure 3: Observations for Elektron 21, a) optical image of surface before fatigue, b) optical image after 522 cycles, c) optical image after failure at 552cycles, d) EBSD map of sample obtained before testing, e) Displacement map between 0 and 522 cycles, f) strain map between 0 and 552 cycles. The same region is marked by a white dotted box in each image. Locations 1-4 in f) are examined in Figure 4.

The localisation of strain is shown more clearly in Figure 5 for WE43 and Figure 6 for Elektron 21. Twinning is observed in a number of grains (marked by arrows both cases). These locations do not necessarily coincide with the regions of higher strain (i.e. Figure 5c and Figure 6c), but do tend to be grains with higher Schmid factors for the $\{10\bar{1}2\}\langle 10\bar{1}0\rangle$ system (i.e. Figure 5d and Figure 6d).

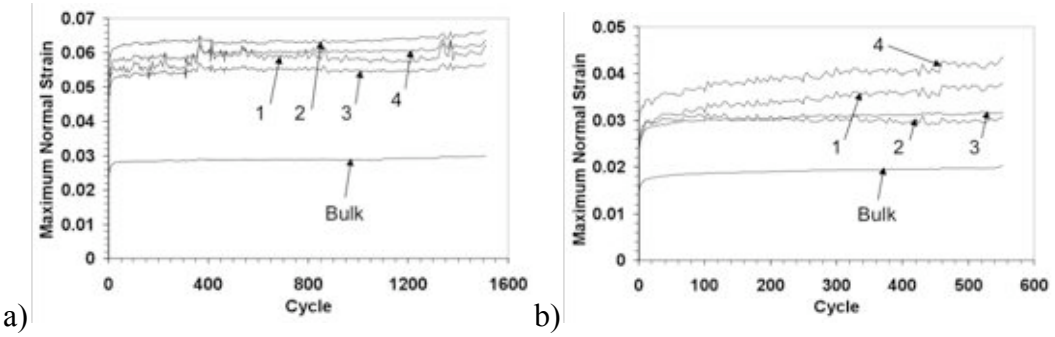

Figure 4: Variation of bulk strain and localised strain at locations 1 to 4 with the number of fatigue cycles, a) WE43, b) Elektron 21. The locations 1 to 4 are labelled in Figure 2 and Figure 3.

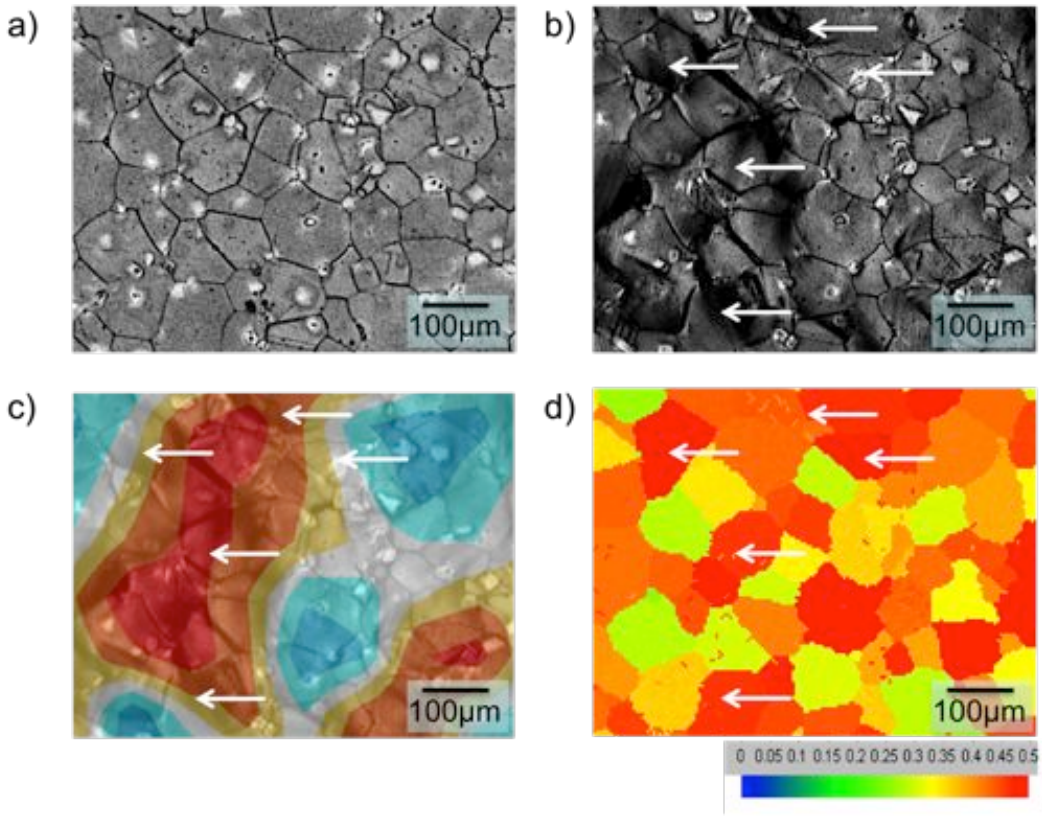

Figure 5: Comparison between deformation, strain map and grain orientation in Elektron WE43, a) optical image at start of test, b) optical image after 1510 cycles, c) strain map between 0 and 1510 cycles (same scale as Figure 2f), d) Schmid factor map for $\{10\bar{1}2\}\langle 10\bar{1}0\rangle$ from EBSD data. The same locations are marked by arrows.

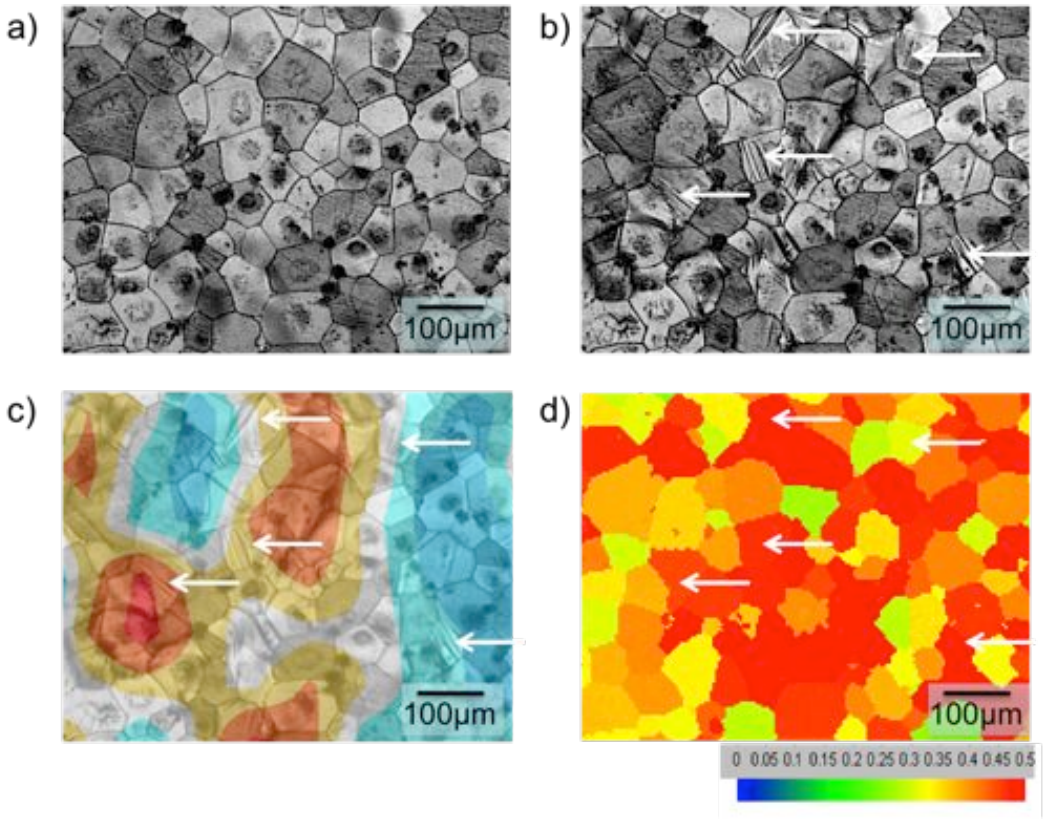

Figure 6: Comparison between deformation, strain map and grain orientation in Elektron 21, a) optical image at start of test, b) optical image after 552 cycles, c) strain map between 0 and 552 cycles (same scale as Figure 3f), d) Schmid factor map for $\{10\bar{1}2\}\langle 10\bar{1}0\rangle$ from EBSD data. The same locations are marked by arrows.

4 DISCUSSION

The goal of this work is to determine whether the distribution of low cycle fatigue damage in cast magnesium alloys can be related to the microstructure, and in particular its heterogeneity. The in-situ observations for both Elektron WE43 and Elektron 21 demonstrate that localised deformation occurs during low cycle fatigue testing. The image correlation analysis has measured the bulk elongation and strain of the samples (Figure 4), and it is concluded that the observed strain localisation is due to heterogeneous plastic deformation in the microstructure. The most significant deformation develops in the first few load cycles, but there is a gradual increase in magnitude of the localised strain regions with cycling. In studies of other materials, crack nucleation has been shown to a cause of apparent strain localisation in strain maps, due to the effect of the crack opening displacement [3] [4]. However, there is no evidence of crack nucleation in these samples prior to failure, and cracking is therefore not considered responsible for the observed strains.

Image correlation has previously been used to observe the localisation of plastic deformation in metals [5]. Such heterogeneity in plastic deformation may arise

from variations in crystal orientation or local hardness. There is clear evidence of twinning (Figure 5 and Figure 6), which is a characteristic deformation mechanism in Magnesium [6]. The twin habit plane in Magnesium is $\{10\bar{1}2\}$ with shear in the $<10\bar{1}0>$ directions. The incidence of observable twinning correlates with some grains in which the resolved shear stress (i.e. Schmid factor) for this system is high. However, optical microscopy can only detect twinning if surface steps are produced, hence it is not unexpected that twins are not observed in all grains with high Schmid factor. Grains with low Schmid factor do not exhibit twinning. A more detailed analysis of the EBSD data, to relate the observed twinning to the physical orientation of the high Schmid factor slip systems, might be done to investigate this further. The objective would be to predict the distribution of twinning grains in the strain-mapped region, and their directions of shear, and hence obtain the distribution of strain by twinning.

The observed regions of higher strain in WE43 and Elektron 21 do not show any obvious correlation with the distribution of twinning, nor the Schmid factor maps. Image correlation measures the two-dimensional displacements parallel to the surface, so it is not unexpected that out-of-surface displacements from twinning are undetected. Similarly, the Schmid factor map does not differentiate between twinning grains that will produce shears parallel or perpendicular to the specimen surface. This could be obtained by more detailed analysis, as discussed above.

The fracture path is associated with regions of high strain that are detected by image correlation. As there are no fatigue crack nuclei detected prior to failure, it is deduced that failure by low cycle fatigue occurs by coalescence of damage. Cracking of intergranular brittle phases due to plastic strain has been observed in WE43 [7], and such cracking is more likely to occur in the regions of localised plastic strain with increasing numbers of cycles, as the magnitude of strain increases. The distribution of damage is thus sensitive to the heterogeneity of plastic deformation, and the distribution of brittle phases in the microstructure. Work is currently in progress, utilising the methods described in this paper, to confirm this and to develop models for the influence of microstructure on the susceptibility to low cycle fatigue damage.

5 CONCLUSION

Image correlation of optical images obtained during low cycle fatigue testing of cast magnesium alloys Elektron WE43 and Elektron 21 shows that localised regions of increase strain develop prior to failure. These influence the fracture path. Although some correlations between observed twinning and grain orientation are apparent, a detailed analysis of grain orientation data will be required in order to correlate the development of the observed surface plastic strains to microstructure. The development of localised plastic strain is proposed to cause damage by cracking of intergranular brittle phases, which then initiates low cycle fatigue failure.

Acknowledgements: AAK is grateful to the Higher Education Commission of Pakistan for supporting his studies at Manchester Univerity. The material was kindly supplied by Magnesium Elektron Ltd. The views expressed in this paper are those of the authors.

6 REFERENCES

[1] S. Schumann, H. Friedrich. Current and future use of magnesium in the automobile industry. Materials Science Forum 419–422 (2003) 51–6

[2] C. Wang, Z. Liu, L. Chen. Low-cycle fatigue behavior of three die cast magnesium alloys Materials Science Forum, 546-549 (2007) 147-150

[3] S. Rahimi, D.L. Engelberg, J.A. Duff and T.J. Marrow. In-situ Observation of Intergranular Crack Nucleation in a Grain Boundary Controlled Austenitic Stainless Steel, J. Microscopy, (2008) *Article in Press*.

[4] M.R. Joyce, T.J. Marrow, P. Mummery and B.J. Marsden. Observation of microstructure deformation and damage in nuclear graphite Engineering Fracture Mechanics, 75 (2008) 3633-3645

[5] J. Quinta da Fonseca, P.M. Mummery and P.J. Withers, Full-field strain mapping by optical correlation of micrographs acquired during deformation, Journal of Microscopy, 218, (2005), 9–21

[6] Munroe, N., and Tan, X., Orientation dependence of slip and twinning in hcp metals, Scripta Materialia, 36, (1997) 1383-8

[7] T.J. Marrow, A Bin Ahmad, I.N Khan, S.M.A. Sim and S. Torkamani, Environment-assisted cracking of cast WE43-T6 magnesium, Materials Science and Engineering A, 387-89 (2004), 419-423